UC Irvine
UC Irvine Previously Published Works

Title
Video-rate mid-infrared imaging in the molecular fingerprint region via nanosecond non-degenerate two-photon absorption

Permalink
https://escholarship.org/uc/item/7647h9nk

Journal
APL Photonics, 11(5)

ISSN
2378-0967

Authors
Garcia, Evan P
Luna-Palacios, Yryx Y
Nguyen, Ryan
et al.

Publication Date
2026-05-01

DOI
10.1063/5.0324530

Copyright Information
This work is made available under the terms of a Creative Commons Attribution License, available at https://creativecommons.org/licenses/by/4.0/

Peer reviewed

eScholarship.org Powered by the California Digital Library
University of California

APL Photonics

RESEARCH ARTICLE | MAY 18 2026

Video-rate mid-infrared imaging in the molecular fingerprint region via nanosecond non-degenerate two-photon absorption

Evan P. Garcia ; Yryx Y. Luna-Palacios ; Ryan Nguyen; Adam Hanninen ; Aleksei I. Noskov ; Eric O. Potma ; Dmitry A. Fishman

Check for updates

APL Photonics 11, 056112 (2026)
https://doi.org/10.1063/5.0324530

View Online
Export Citation

Articles You May Be Interested In

High spectral resolution mid-infrared hyperspectral computational ghost imaging enabled by wavelength-tunable nonlinear structured illumination

APL Photonics (October 2026)

06 November 2026 21:33:27

AMERICAN ELEMENTS
THE MATERIALS SCIENCE MANUFACTURER®
Now Invent.™
29th ANNIVERSARY 1997 – 2026

American Elements Opens a World of Possibilities
...Now Invent!
www.americanelements.com
© 1997-2026. American Elements is a U.S. Registered Trademark

AIP Publishing

Video-rate mid-infrared imaging in the molecular fingerprint region via nanosecond non-degenerate two-photon absorption

Cite as: APL Photon. 11, 056112 (2026); doi: 10.1063/5.0324530
Submitted: 25 January 2026 • Accepted: 30 April 2026 •
Published Online: 18 May 2026

View Online Export Citation CrossMark

Evan P. Garcia,[1] Yryx Y. Luna-Palacios,[2] Ryan Nguyen,[1] Adam Hanninen,[3] Aleksei I. Noskov,[1] Eric O. Potma,[1,2,a)] and Dmitry A. Fishman[1,b)]

AFFILIATIONS

[1] Department of Chemistry, University of California Irvine, Irvine, California 92697, USA
[2] Beckman Laser Institute and Medical Clinic, University of California Irvine, Irvine, California 92697, USA
[3] Trestle Optics, Irvine, California 92697, USA

[a)] epotma@uci.edu
[b)] Author to whom correspondence should be addressed: dmitryf@uci.edu

ABSTRACT

Non-degenerate two-photon absorption (NTA) offers an attractive route for wide-field mid-infrared imaging by mapping long wavelength information into the spectral detection windows of mature near-infrared detector technologies. However, existing NTA implementations rely almost exclusively on complex, large-footprint femtosecond laser systems, severely limiting practicality and scalability. Here, we demonstrate an NTA imaging platform that replaces the ultrafast laser with a compact nanosecond mid-IR source coupled to a high-definition indium gallium arsenide camera. Operating in the nanosecond regime removes stringent temporal-overlap requirements, dramatically simplifying system architecture while preserving high detection sensitivity. Using this approach, we achieve chemically selective, wide-field imaging deep into the mid-IR molecular fingerprint region and demonstrate, for the first time, video-rate NTA imaging in this spectrally rich regime. By combining relaxed alignment constraints, compact excitation, and high-speed fingerprint-region imaging, this work establishes nanosecond NTA as a practical and scalable foundation for next-generation mid-IR chemical imaging.

© 2026 Author(s). All article content, except where otherwise noted, is licensed under a Creative Commons Attribution (CC BY) license (https://creativecommons.org/licenses/by/4.0/). https://doi.org/10.1063/5.0324530

06 November 2026 21:33:27

INTRODUCTION

The mid-infrared (mid-IR) spectral region (3–12 μm) hosts a rich set of fundamental vibrational resonances that provide intrinsic chemical contrast for applications spanning medicine,[1,2] biology,[3] manufacturing,[4,5] and defense.[6] Despite its importance, practical mid-IR imaging remains limited by the trade-offs associated with existing detection strategies. Direct detection with mid-IR cameras offers broad spectral coverage but is constrained by cost, limited pixel numbers, or low frame rates.[7,8] Furthermore, the small bandgaps of mid-IR detector materials result in high thermal noise, often necessitating cryogenic cooling to achieve acceptable performance.[9,10]

Recent approaches seek to circumvent the fundamental challenges of mid-IR detection and imaging by mapping mid-IR spectral information into the near-infrared or visible domains, where detection technologies are significantly more efficient, mature, and readily available.[11–20] One such approach exploits non-degenerate two-photon absorption (NTA), in which a mid-IR photon is combined in time and space with a higher-energy visible or near-infrared photon to directly induce an interband optical transition in the semiconductor sensor material.[13,21] This mechanism enables the use of wide-bandgap semiconductor detectors and focal plane arrays based on well-established platforms, such as silicon (Si) and indium gallium arsenide (InGaAs), which offer superior performance compared to conventional mid-IR detectors, particularly in terms of

© Author(s) 2026

reduced thermal noise, higher pixel density, and operational stability. By leveraging these mature detection technologies, NTA-based mid-IR imaging overcomes many of the intrinsic limitations of traditional mid-IR cameras and focal plane arrays.[22,23] Importantly, as a χ^3-mediated nonlinear absorption process, NTA does not require phase matching, it accommodates an ultrabroad spectral range across the near-to-far IR, and it does not rely on complex image reconstruction. These attributes significantly simplify implementation and enhance robustness against environmental drift and external perturbations. Leveraging these advantages, NTA-based mid-IR (MIR) imaging modalities have enabled high-speed chemically selective high-definition imaging,[22,24] high-speed hyperspectral imaging,[25] and volumetric chemically selective imaging.[26]

Despite addressing several fundamental challenges in mid-IR imaging, detectable NTA signals generated in the thin semiconductor layers (<30 μm well thickness) of modern camera sensors require optical irradiances substantially higher than those used in linear detection schemes. As a result, most existing demonstrations rely on ultrafast femtosecond or picosecond laser sources, whose large footprint, high cost, and operational complexity limit the applicability of NTA imaging outside specialized optical laboratories.[23–25] Advancing NTA toward practical and deployable MIR imaging systems, therefore, necessitates the development of more compact and accessible excitation sources.

In this work, we address the complexity of light sources typically required for NTA by demonstrating an imaging platform based on a compact nanosecond light source that provides both the MIR excitation and the near-infrared gate pulse. This approach represents a critical step toward bridging the gap between proof-of-principle demonstrations and practical applications. In addition to lower cost and reduced footprint, a key advantage of nanosecond excitation over femtosecond sources is the relaxation of maintaining the sensitive temporal overlap between the mid-IR and gate pulses. Because nanosecond pulses are orders of magnitude longer in duration, temporal overlap is readily maintained over standard optical path lengths, significantly simplifying experimental implementation. Using a compact optical parametric oscillator (OPO) pumped by a nanosecond laser, we achieve high-speed, wide-field mid-IR imaging across the MIR molecular fingerprint region. We demonstrate chemically specific contrast in both macroscopic and microscopic imaging modes, including real-time, video-rate analysis of bio-relevant materials. These results establish that more

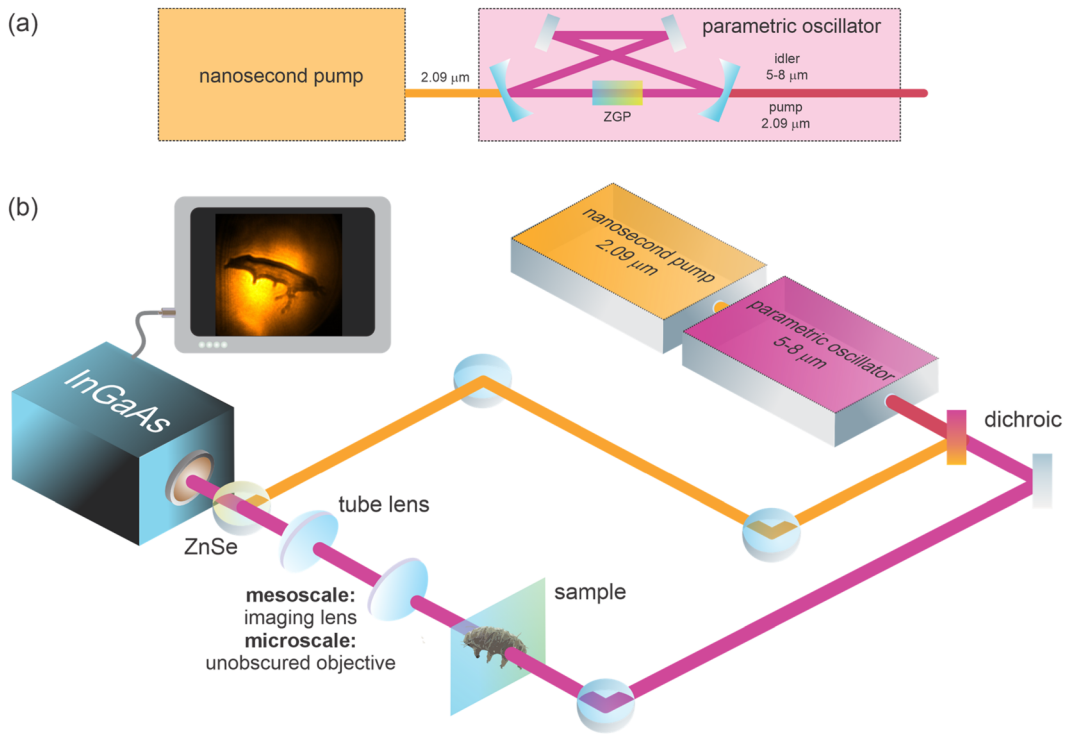


FIG. 1. (a) Schematic of a nanosecond Ho:YAG laser (2.09 μm) seeding a compact $ZnGeP_2$ (ZGP)-based optical parametric oscillator (OPO) to generate tunable mid-infrared idler pulses spanning the molecular fingerprint region (≈60 ns pulse duration, 10 W, 1 kHz repetition rate). While the OPO design supports broad tunability from ~2.6 to 10 μm, the experiments reported here were performed in the pre-characterized 5–8 μm spectral range. (b) Nanosecond non-degenerate two-photon absorption (ns-NTA) imaging setup, in which the tunable mid-IR idler serves as the excitation beam and the residual 2.09 μm pump pulse acts as the gate pulse. The two beams are spatially and temporally recombined on an InGaAs camera (MVCam, Princeton Infrared Technologies Inc.; 1280 × 1020 pixels, 12 μm pixel pitch, 0.73 eV bandgap). Two imaging configurations were employed: mesoscale imaging using a 75 mm CaF_2 lens (NA = 0.015) and microscale imaging using a custom-designed, unobscured reflective objective (NA = 0.65).[30]

06 November 2026 21:33:27

© Author(s) 2026

affordable nanosecond excitation can efficiently drive NTA-based detection in the mid-IR fingerprint region using compact sources and standard detectors, providing a viable pathway toward practical, scalable MIR imaging systems.

MATERIALS AND METHODS

Sample preparation

Polymer samples were melted, deposited onto 5 mm-thick NaCl windows, and pressed flat using a CaF_2 coverslip. L-proline crystals were mounted on IR-transparent KBr windows. Type I collagen from rat tail tendon was flattened, mounted on CaF_2 microscope slides, and sealed with a CaF_2 coverslip. Tardigrades were pipetted from an aqueous suspension, allowed to dry under ambient conditions, and sealed beneath a CaF_2 coverslip.

FTIR analysis

Infrared absorption spectra were acquired using a Jasco 4700 FTIR spectrometer equipped with a diamond-based attenuated total reflection (ATR) accessory. Spectra were collected with a 2 cm^{-1} resolution and averaged over 16 scans. Tardigrade spectra were obtained with a Nicolet iS20 FTIR spectrometer coupled to a Thermo Scientific Nicolet Continuum microscope using a confocal Reflachromat 15×, 0.58 NA objective. Data were collected with a resolution of 2 cm^{-1} and averaged over 16 scans.

Tunable nanosecond light source

For ns-NTA excitation, we developed a zinc germanium phosphide ($ZnGeP_2$) optical parametric oscillator (OPO) configured for type-I phase matching. $ZnGeP_2$ was selected for its large nonlinear coefficient (~75 pm/V) and favorable thermal properties, enabling broad, continuous mid-infrared tunability spanning 2.5–10 μm, encompassing both the signal and idler beams.[27,28] The OPO was pumped by a Q-switched Ho:YAG laser (2090 nm, 45 ns pulses, 1 kHz, 10 W average power; HLPN 2090, IPG) and implemented in a compact X-shaped confocal resonator ring cavity (L = 60 cm), resonant with the signal beam, with two concave intra-cavity mirrors (radius of curvature R = 100 mm) and a partially transmitting output coupler.[29]

NTA setup

A schematic of the experimental setup is shown in Fig. 1. The idler output of the OPO, separated from the residual pump using a custom dichroic mirror (2090 nm cutoff), was pre-calibrated and spectrally characterized over the 5–7 μm range and served as the MIR light source in the imaging experiments. The residual 2.09 μm OPO pump radiation was spatially and temporally overlapped with the tunable MIR idler beam to generate a non-degenerate two-photon absorption signal directly on the InGaAs camera chip (bandgap 0.73 eV, 1280 × 1020 pixels, 12 μm pixel pitch; MVCam, Princeton Infrared Technologies). The MIR beam was delivered through an imaging system composed of either

06 November 2026 21:33:27

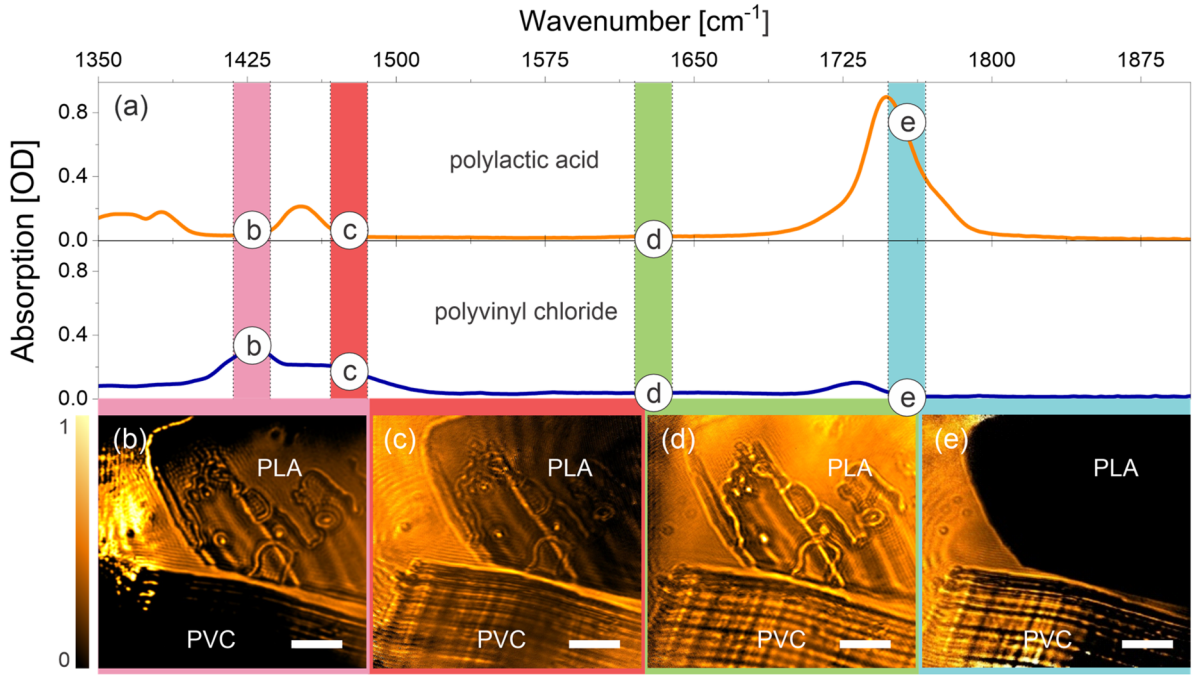


FIG. 2. Static mesoscale ns-NTA imaging. (a) FTIR absorption spectra of polylactic acid (PLA, orange) and polyvinyl chloride (PVC, blue) polymers in a hybrid sample. [(b)–(e)] Wide-field mid-IR images acquired at selected spectral points indicated in (a). The images show strong absorption contrast consistent with the characteristic vibrational features of each polymer. Scale bar: 1 mm. Exposure time: 30 ms. All images are normalized and corrected for small variations in excitation power.

© Author(s) 2026

a 2× magnification CaF_2 telescope or an unobscured all-reflective objective (NA = 0.65) paired with a CaF_2 tube lens (f = 150 mm). The resulting pulse irradiance at the camera chip was set to 217 W cm^{-2} for the MIR beam and 263 W cm^{-2} for the 2.09 μm gate radiation. The nanosecond laser and OPO system used in this work have approximate dimensions of ~25 × 20 cm^2 each, resulting in a setup with a compact overall footprint.

RESULTS

Static mesoscale imaging in the molecular fingerprint range

To demonstrate the potential of nanosecond NTA (ns-NTA) imaging in the molecular fingerprint region and to achieve label-free, chemically selective contrast, we examined a variety of organic samples. For these mesoscale imaging experiments, a twofold expansion of the MIR beam was used to match the beam size to the camera chip area (~1.9 cm^2). As an initial demonstration, we investigated a hybrid sample consisting of two adjacent thin polymer films: polylactic acid (PLA) and polyvinyl chloride (PVC). Figure 2(a) shows the FTIR spectra of PLA and PVC, with specific spectral points marked, where ns-NTA imaging was performed [Figs. 2(b)–2(g)]. Consistent with the infrared absorption spectra of each polymer, the NTA images reveal clear chemical contrast at selected frequencies. For example, the PVC material appears dark due to strong absorption at 1420 cm^{-1} [Fig. 2(b)], whereas the transmission contrast is reversed at 1760 cm^{-1} owing to strong absorption by PLA [Fig. 2(f)]. All NTA images in Fig. 2 were normalized and corrected for small variations in excitation power.

Dynamic imaging in the fingerprint range

Further demonstration of the ns-NTA capability was performed using L-proline, a common amino acid involved in key cellular and metabolic processes and essential for protein synthesis. The absorption spectrum of crystalline L-proline is shown in Fig. 3(a), highlighting a characteristic resonance associated with the carbonyl stretching mode at 1560 cm^{-1}. Following the absorption spectrum, Fig. 3 presents static mesoscale ns-NTA images of crystalline L-proline clusters acquired on-resonance [1560 cm^{-1}, Fig. 3(b)] and off-resonance [1800 cm^{-1}, Fig. 3(c)]. To demonstrate chemically selective dynamic imaging in the fingerprint region, we

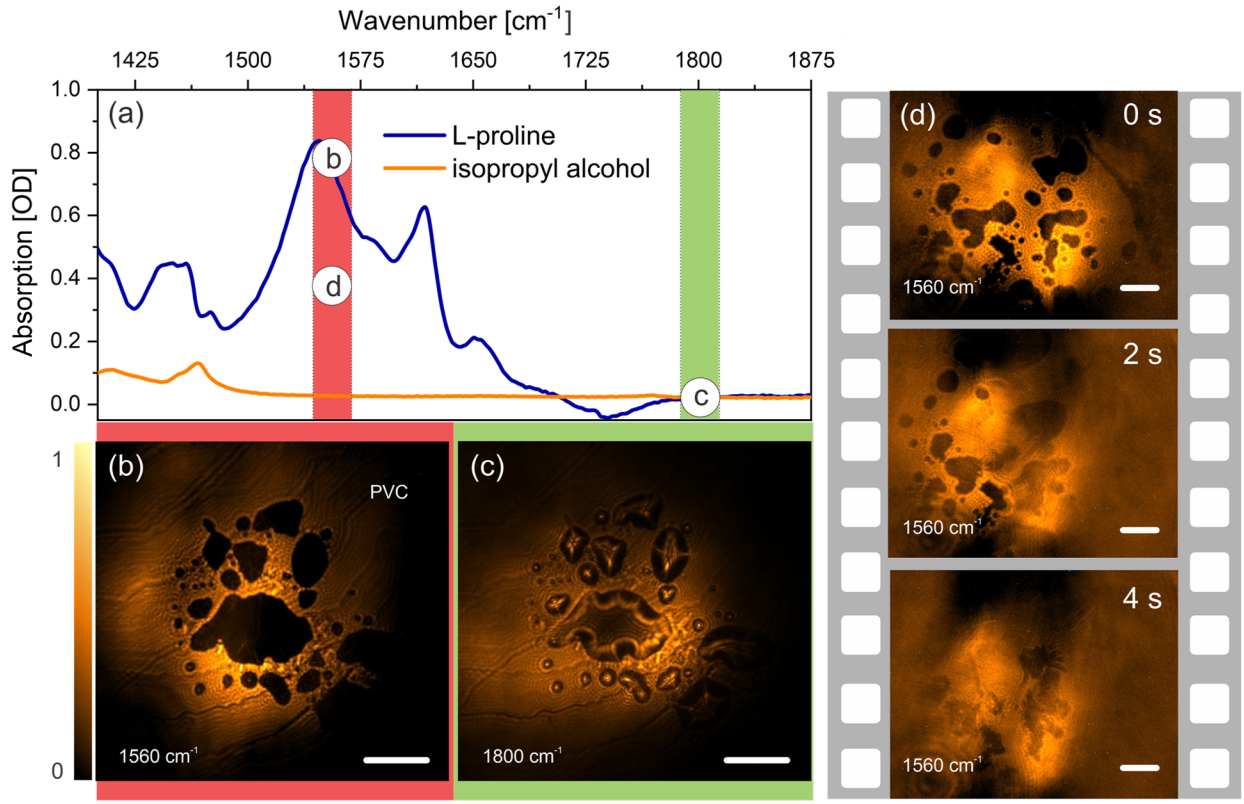


FIG. 3. Dynamic imaging in the mid-IR fingerprint region. (a) FTIR absorption spectra of L-proline (blue) and isopropyl alcohol (IPA, orange). [(b) and (c)] Representative wide-field ns-NTA images acquired on-resonance with the carbonyl stretching mode (1560 cm^{-1}) and off-resonance (1800 cm^{-1}), respectively, showing clear absorption contrast. Scale bar: 1 mm. Exposure time: 30 ms. (d) Snapshot from a time-resolved ns-NTA video visualizing the dissolution of L-proline clusters in real time, recorded at 33 frames/s at the carbonyl stretching resonance (Multimedia available online). The video reveals cluster dissolution through concurrent changes in morphology and local absorption contrast.

06 November 2026 21:33:27

© Author(s) 2026

recorded a video of L-proline crystals dissolving in isopropanol alcohol (IPA). The video shows that the crystalline amino-acid clusters dissolve within a few seconds, while simultaneously revealing both the evolving cluster morphology and a pronounced change in absorption contrast as solvation alters the local L-proline concentration. This high-definition (~1.2 Mpx) video was recorded at ~33 f/s (30 ms per frame) and is presented in Fig. 3 (Multimedia available online).

Microscale imaging of collagen and micro-organisms

To extend NTA-based mid-IR imaging to the microscale, we employed a setup incorporating a custom-designed, unobscured, all-reflective microscope objective [Fig. 4(a)]. The objective design and its characterization for both linear and nonlinear imaging have been described previously.[30] As representative microscale samples, we investigated rat tail collagen tissue and a tardigrade (*Milnesium tardigradum*), a microscopic organism commonly found in aqueous environments. Figure 4(a) shows the FTIR spectra of both samples, highlighting the characteristic amide I absorption band near 1650 cm^{-1}.

Figures 4(b) and 4(c) (rat tail collagen) and Figs. 4(d) and 4(e) (tardigrade) present ns-NTA images acquired on- and off-resonance using two spectral points: the amide I resonance at 1650 cm^{-1} and an off-resonant reference at 1800 cm^{-1}. Figures 4(f) and 4(g) show the corresponding composite images, in which regions exhibiting resonant absorption are rendered in red, while spectrally transparent regions appear yellow, forming false-color mid-IR images of the biological samples. All images exhibit clear and well-defined absorption contrast with acquisition times as short as 30 ms, demonstrating that ns-NTA can be extended to microscopic length scales while preserving both chemical specificity in the molecular fingerprint region and high imaging speed. We note that the ns-NTA fingerprint image of the tardigrade was acquired on a dehydrated (non-living)

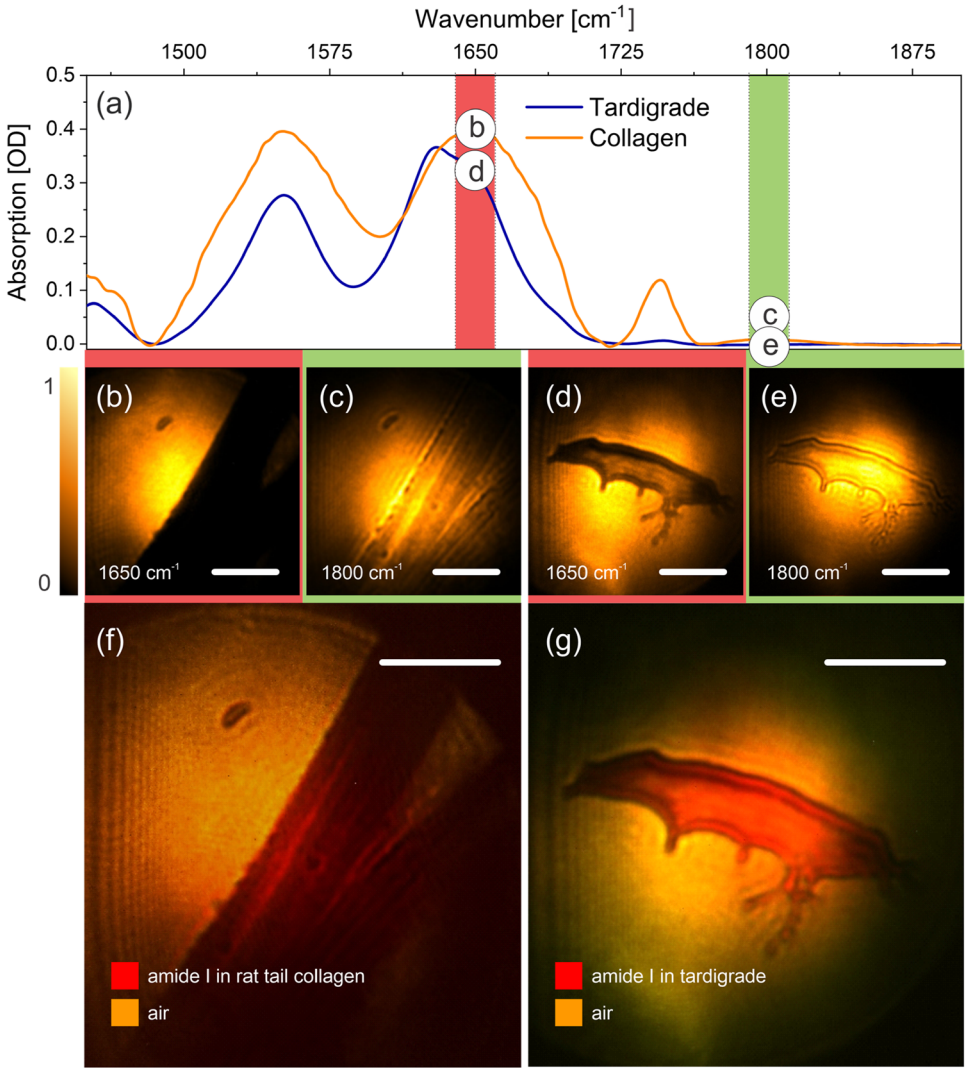


FIG. 4. (a) FTIR absorption spectra of rat tail collagen (blue) and dehydrated tardigrade (*Milnesium tardigradum*, orange). Both spectra exhibit a pronounced absorption feature near 1650 cm^{-1}, corresponding to the amide I vibrational band. [(b)–(e)] ns-NTA images acquired on- and off-resonance of the amide I band for collagen [(b) and (c)] and tardigrade [(d) and (e)]. Scale bar is 100 μm, and exposure time was 30 ms. [(f) and (g)] Corresponding false-color composite images constructed from the on- and off-resonance image pairs for collagen (f) and tardigrade (g). Scale bar is 100 μm. Regions exhibiting amide I absorption are rendered in red, while areas with negligible absorption appear yellow.

06 November 2026 21:33:27

© Author(s) 2026

specimen. Although tardigrades are exceptionally resilient—capable of surviving extreme environments, including exposure to outer space—maintaining a living and motile organism requires an aqueous environment. For relatively large and optically thick living specimens, strong mid-IR absorption by water fundamentally limits its photon transmission in the fingerprint region, imposing practical constraints on chemically specific imaging under hydrated conditions. Under dehydrated conditions, however, ns-NTA imaging at 1650 cm^{-1} yields clear vibrational contrast associated with protein-rich structures, with acquisition times comparable to those used for collagen [Figs. 4(d) and 4(g)].

Taken together, these results establish that ns-NTA enables chemically specific mid-IR imaging at microscopic length scales within the molecular fingerprint region, while maintaining short acquisition times compatible with dynamic measurements. This capability extends NTA beyond previously demonstrated mesoscale implementations and confirms that nanosecond-driven excitation can support high-speed, label-free vibrational imaging of biological specimens with microscale spatial resolution.

DISCUSSION

The results presented here reposition non-degenerate two-photon absorption as a practical and scalable strategy for mid-infrared imaging, rather than a technique confined to ultrafast optics laboratories. By demonstrating NTA driven entirely by nanosecond excitation, this work reduces the complexity, cost, and footprint of NTA-based imaging systems, while also enabling portability and mobility. In contrast to previous implementations relying on femtosecond or picosecond laser sources,[22,24–26] the nanosecond platform presented here is readily compatible with standard laboratory environments and is amenable to miniaturization. Ongoing advances in compact nanosecond light sources suggest a clear pathway toward future field-deployable implementations. This transition directly addresses one of the central bottlenecks that has limited the broader adoption of NTA imaging despite its intrinsic advantages.

We note that several commercially available mid-infrared imaging approaches exist that rely on either direct or indirect detection of mid-IR photons. The direct methods broadly include wide-field detection using focal plane array detectors, such as microbolometer-[31] or MCT-based systems,[32,33] which typically offer array sizes on the order of ~480 × 480 pixels or ~128 × 128 pixels, respectively. While these methods achieve high-speed imaging within a single field of view, mapping larger areas or acquiring higher-definition images typically requires mosaicking strategies, introducing trade-offs in acquisition speed. In parallel, QCL-enabled point-scanning imaging approaches have been developed using single-element detectors. In these discrete frequency infrared (DFIR) implementations, spectral mapping is achieved by sequentially acquiring frames at different frequency settings.[33–36] Such approaches can offer improved signal-to-noise ratio and reduced susceptibility to coherence-related artifacts. These systems can achieve competitive sensitivity at high acquisition speeds.[34] However, this typically comes at the expense of increased system complexity, involving scanning optics and the need for sequential acquisition across the field of view. As a result, a fundamental trade-off emerges between pixel dwell time, achievable SNR, and overall imaging speed, particularly for large-area or high-definition measurements.[33] Among the indirect IR imaging methods, photothermal infrared imaging approaches stands out as prominent example,[17,37,38] which provide an alternative contrast mechanism based on thermally induced changes following mid-infrared absorption.

In contrast, ns-NTA combines some advantages of these techniques by taking advantage of parallel detection afforded by the wide-field detection configuration, while utilizing >1 Mpx near-IR camera formats that enable rapid high-definition imaging. From a system perspective, direct MIR imaging typically combines compact light sources with specialized detectors, where performance and cost are closely linked to detector characteristics, whereas ns-NTA solves the detection challenge by employing mature large-format detector technologies. Earlier NTA-based IR imaging, however, relied on ultrafast pulses to boost performance, at the expense of increased excitation complexity. The nanosecond implementation, on the other hand, points toward simpler and more accessible excitation sources, including high-brightness quasi-continuous-wave systems.

In ultrafast NTA implementations, femtosecond pulse durations necessitate precise delay-line control and continuous optimization to maintain temporal overlap between the mid-IR and gate pulses. In the nanosecond regime, pulse durations are sufficiently long that temporal overlap is effectively guaranteed once spatial overlap is achieved. As a result, NTA becomes a geometrically rather than temporally constrained process. This dramatically simplifies system alignment, enhances long-term stability, and renders the optical layout highly forgiving to environmental drift. Importantly, this relaxed timing constraint opens pathways that are impractical for ultrafast systems, including the use of optical fibers, flexible beam delivery, and compact or modular architectures, all of which are essential for deployable and user-friendly mid-IR imaging platforms.

An important implication of operating in the nanosecond regime is that relaxed temporal and high irradiance expand compatibility with emerging mid-IR light sources that are otherwise incompatible with ultrafast NTA implementations. In particular, quantum cascade lasers (QCLs) offer compact form factors, intrinsic mid-IR emission, and rapid electronic tunability that is well-suited for hyperspectral imaging. While current commercially available QCL sources generally do not yet provide sufficient peak irradiance to reliably drive NTA in standard camera sensors, the relaxed temporal constraints of ns-NTA make QCL integration a realistic long-term pathway rather than a conceptual mismatch. Continued advances in high-peak-power QCL designs,[39] along with detector architectures optimized for nonlinear absorption, could enable solid-state NTA imaging platforms with rapid wavelength agility.

Crucially, the gains of ns-NTA simplicity do not necessarily come at the expense of performance. While previous femtosecond NTA implementations[13,24–26] benefited from higher peak irradiances on the order of MW/cm^2, we were able to offset the lower ns irradiances by increasing the average power and signal integration time. The resulting average powers of several tens of mW (irradiance of several hundreds of W/cm^2) and 30 ms camera integration times yielded comparable NTA signals while retaining video rate acquisition rates. Using these settings, nanosecond-driven NTA achieves chemically specific imaging deep into the molecular fingerprint region, representing the first realization of NTA imaging in

06 November 2026 21:33:27

© Author(s) 2026

this spectrally rich regime. This result highlights a defining strength of NTA as a χ(3)-mediated process: its intrinsic lack of phase-matching constraints enables seamless and *gapless spectral coverage extending from the near-infrared into the mid- and, in principle, far-infrared using a single camera chip*.[40] Furthermore, the increase in photon energy disparity enhances the NTA response,[41] directly benefiting operation in the fingerprint region, where vibrational resonances are strongest. This behavior underscores the fundamental scalability of NTA and distinguishes it from alternative frequency-conversion approaches that rely on separate nonlinear crystals and strict phase-matching conditions.[42,43]

Beyond spectral reach, the ns-NTA platform enables high-speed, wide-field imaging with acquisition times short enough to exceed standard video rates. This capability is particularly significant given that fingerprint-region imaging is traditionally associated either with slow point-scanning modalities or with limited availability of high-definition focal plane arrays sensitive in this spectral range. While performance in aqueous environments remains constrained by mid-IR attenuation in water, the demonstrated acquisition speeds establish that, where optical transmission permits, wide-field nanosecond NTA allows chemically selective imaging with millisecond-scale frame times, enabling the observation of dynamic chemical and physical processes in real time.

CONCLUSIONS

This work establishes nanosecond-driven non-degenerate two-photon absorption as a practically distinct and scalable implementation of mid-infrared imaging. By eliminating ultrafast timing constraints, ns-NTA decouples chemical specificity and spectral reach from system complexity, enabling compact, robust, and intrinsically mobile imaging architectures without sacrificing performance. The demonstration of wide-field, video-rate imaging in the molecular fingerprint region highlights the capability of ns-NTA to access vibrational contrast with substantially greater simplicity than previous NTA implementations, while maintaining comparable nonlinear signal levels. Together, these results define a new design space for NTA-based imaging systems and provide a clear pathway toward deployable mid-IR chemical imaging technologies.

ACKNOWLEDGMENTS

D.A.F. thanks Yulia Davydova for support and help during this study. D.A.F. and E.O.P. acknowledge funding from the Chan Zuckerberg Initiative under Grant No. 2023-321174 (5022), GB-1585590, and from NSF under Grant No. ECCS–2434622. A.H. acknowledges NIH under Grant No. R43GM149004.

AUTHOR DECLARATIONS

Conflict of Interest

A.H. declares a financial interest in Trestle Optics. All other authors declare no competing interest.

Author Contributions

Evan P. Garcia: Conceptualization (equal); Data curation (equal); Formal analysis (equal); Funding acquisition (equal); Investigation (equal); Methodology (equal); Project administration (equal); Resources (equal); Supervision (equal); Validation (equal); Visualization (equal); Writing – original draft (equal); Writing – review & editing (equal). **Yryx Y. Luna-Palacios**: Conceptualization (equal); Data curation (equal); Formal analysis (equal); Investigation (equal); Methodology (equal); Project administration (equal); Validation (equal); Visualization (equal); Writing – original draft (equal); Writing – review & editing (equal). **Ryan Nguyen**: Conceptualization (equal); Data curation (equal); Formal analysis (equal); Investigation (equal); Methodology (equal); Project administration (equal); Resources (equal); Validation (equal); Visualization (equal); Writing – original draft (equal); Writing – review & editing (equal). **Adam Hanninen**: Formal analysis (equal); Investigation (equal); Methodology (equal); Resources (equal); Validation (equal); Visualization (equal); Writing – review & editing (equal). **Aleksei I. Noskov**: Conceptualization (equal); Formal analysis (equal); Investigation (equal); Methodology (equal); Resources (equal); Writing – review & editing (equal). **Eric O. Potma**: Conceptualization (equal); Data curation (equal); Formal analysis (equal); Funding acquisition (equal); Investigation (equal); Methodology (equal); Project administration (equal); Resources (equal); Supervision (equal); Validation (equal); Visualization (equal); Writing – review & editing (equal). **Dmitry A. Fishman**: Conceptualization (equal); Data curation (equal); Formal analysis (equal); Funding acquisition (equal); Investigation (equal); Methodology (equal); Project administration (equal); Resources (equal); Supervision (equal); Validation (equal); Visualization (equal); Writing – review & editing (equal).

DATA AVAILABILITY

The data that support the findings of this study are available from the corresponding author upon reasonable request.

REFERENCES

[1] T. Yin, T. Yang, X. Dong, B. Liu, and Z. Qiao, "Mid-infrared spectroscopy and its applications in biomedical analysis and imaging," Biochem. Biophys. Res. Commun. **790**, 152890 (2025).

[2] E. Willenbacher *et al.*, "Application of mid-infrared microscopic imaging for the diagnosis and classification of human lymphomas," J. Biophot. **14**, e202100079 (2021).

[3] Q. Xia, J. Yin, Z. Guo, and J. X. Cheng, "Mid-infrared photothermal microscopy: Principle, instrumentation, and applications," J. Phys. Chem. B **126**, 8597–8613 (2022).

[4] S. Primpke, M. Godejohann, and G. Gerdts, "Rapid identification and quantification of microplastics in the environment by quantum cascade laser-based hyperspectral infrared chemical imaging," Environ. Sci. Technol. **54**, 15893–15903 (2020).

[5] M. Tazreiter, P. Christian, R. Schennach, T. Grießer, and A. M. Coclite, "Simple method for the quantitative analysis of thin copolymer films on substrates by infrared spectroscopy using direct calibration," Anal. Methods **9**, 5266–5273 (2017).

[6] M. A. Butt, M. Juchniewicz, M. Słowikowski, Ł. Kozłowski, and R. Piramidowicz, "Mid-infrared photonic sensors: Exploring fundamentals, advanced materials, and cutting-edge applications," Sensors **25**, 1102 (2025).

[7] F. Hou *et al.*, "Review on infrared imaging technology," Sustainability **14**, 11161 (2022).

[8] S. Bianconi and H. Mohseni, "Recent advances in infrared imagers: Toward thermodynamic and quantum limits of photon sensitivity," Rep. Prog. Phys. **83**, 044101 (2020).

06 November 2026 21:33:27

© Author(s) 2026

[9]A. Rogalski, "Scaling infrared detectors-status and outlook," Rep. Prog. Phys. **85**, 126501 (2022).
[10]A. Rogalski, M. Kopytko, W. Hu, and P. Martyniuk, "Infrared HOT photodetectors: Status and outlook," Sensors **23**, 7564 (2023).
[11]A. Hayat, P. Ginzburg, and M. Orenstein, "Infrared single-photon detection by two-photon absorption in silicon," Phys. Rev. B **77**, 125219 (2008).
[12]H. S. Pattanaik, M. Reichert, D. J. Hagan, and E. W. Van Stryland, "Three-dimensional IR imaging with uncooled GaN photodiodes using nondegenerate two-photon absorption," Opt. Express **24**, 1196–1205 (2016).
[13]D. A. Fishman *et al.*, "Sensitive mid-infrared detection in wide-bandgap semiconductors using extreme non-degenerate two-photon absorption," Nat. Photonics **5**, 561–565 (2011).
[14]E. S. Lee and J. Y. Lee, "High resolution cellular imaging with nonlinear optical infrared microscopy," Opt. Express **19**, 1378–1384 (2011).
[15]T. A. Johnson and S. A. Diddams, "Mid-infrared upconversion spectroscopy based on a Yb:fiber femtosecond laser," Appl. Phys. B **107**, 31–39 (2012).
[16]P. Tidemand-Lichtenberg, J. S. Dam, H. V. Andersen, L. Høgstedt, and C. Pedersen, "Mid-infrared upconversion spectroscopy," J. Opt. Soc. Am. B **33**, D28–D35 (2016).
[17]D. Zhang *et al.*, "Depth-resolved mid-infrared photothermal imaging of living cells and organisms with submicrometer spatial resolution," Sci. Adv. **2**, e1600521 (2016).
[18]S. Junaid *et al.*, "Mid-infrared upconversion based hyperspectral imaging," Opt. Express **26**, 2203–2211 (2018).
[19]S. Junaid *et al.*, "Video-rate, mid-infrared hyperspectral upconversion imaging," Optica **6**, 702–708 (2019).
[20]J. Shi *et al.*, "High-resolution, high-contrast mid-infrared imaging of fresh biological samples with ultraviolet-localized photoacoustic microscopy," Nat. Photonics **13**, 609–615 (2019).
[21]C. M. Cirloganu *et al.*, "Extremely nondegenerate two-photon absorption in direct-gap semiconductors [invited]," Opt. Express **19**, 22951–22960 (2011).
[22]D. Knez, A. M. Hanninen, R. C. Prince, E. O. Potma, and D. A. Fishman, "Infrared chemical imaging through non-degenerate two-photon absorption in silicon-based cameras," Light: Sci. Appl. **9**, 125 (2020).
[23]J. Fang *et al.*, "Single-photon infrared imaging with a silicon camera based on long-wavelength-pumping two-photon absorption," IEEE J. Sel. Top. Quantum Electron. **28**, 3801107 (2022).
[24]E. O. Potma *et al.*, "High-speed 2D and 3D mid-IR imaging with an InGaAs camera," APL Photonics **6**, 096108 (2021).
[25]D. Knez *et al.*, "Spectral imaging at high definition and high speed in the mid-infrared," Sci. Adv. **8**, eade4247 (2022).
[26]E. O. Potma *et al.*, "Rapid chemically selective 3D imaging in the mid-infrared," Optica **8**, 995–1002 (2021).
[27]K. L. Vodopyanov, F. Ganikhanov, J. P. Maffetone, I. Zwieback, and W. Ruderman, "$ZnGeP_2$ optical parametric oscillator with 3.8–12.4-μm tunability," Opt. Lett. **25**, 841–843 (2000).
[28]F. Ganikhanov, T. Caughey, and K. L. Vodopyanov, "Narrow-linewidth middle-infrared $ZnGeP_2$ optical parametric oscillator," J. Opt. Soc. Am. B **18**, 818 (2001).
[29]B. R. Zhao *et al.*, "231 W dual-end-pumped Ho:YAG MOPA system and its application to a mid-infrared ZGP OPO," Opt. Lett. **43**, 5989–5992 (2018).
[30]Y. Y. Luna Palacios *et al.*, "Nonlinear optical microscopy with an obscuration-free, freeform reflective objective," Biomed. Opt. Express **16**, 4530–4540 (2025).
[31]B. Bird and J. Rowlette, "High definition infrared chemical imaging of colorectal tissue using a spero QCL microscope," Analyst **142**, 1381–1386 (2017).
[32]T. P. Wrobel and R. Bhargava, "Infrared spectroscopic imaging advances as an analytical technology for biomedical sciences," Anal. Chem. **90**, 1444–1463 (2018).
[33]Y. Phal, K. Yeh, and R. Bhargava, "Design considerations for discrete frequency infrared microscopy systems," Appl. Spectrosc. **75**, 1067–1092 (2021).
[34]K. Yeh, D. Lee, and R. Bhargava, "Multicolor discrete frequency infrared spectroscopic imaging," Anal. Chem. **91**, 2177–2185 (2019).
[35]K. Yeh and R. Bhargava, "Discrete frequency infrared imaging using quantum cascade lasers for biological tissue analysis," Proc. SPIE **9704**, 970406 (2016).
[36]S. Tiwari *et al.*, "Towards translation of discrete frequency infrared spectroscopic imaging for digital histopathology of clinical biopsy samples," Anal. Chem. **88**, 10183–10190 (2016).
[37]E. S. Lee and J. Y. Lee, "High resolution cellular imaging with nonlinear optical infrared microscopy," Opt. Express **19**, 1378–1384 (2011).
[38]P. D. Samolis and M. Y. Sander, "Phase-sensitive lock-in detection for high-contrast mid-infrared photothermal imaging with sub-diffraction limited resolution," Opt. Express **27**, 2643–2655 (2019).
[39]M. Razeghi, Y. Bai, and F. Wang, "High-power, high-wall-plug-efficiency quantum cascade lasers with high-brightness in continuous wave operation at 3–300 μm," Light: Sci. Appl. **14**, 252 (2025).
[40]H. Ma *et al.*, "Mid-infrared single-pixel imaging via two-photon optical encoding," PhotoniX **6**, 34 (2025).
[41]D. L. Wetzel and S. M. LeVine, "Imaging molecular chemistry with infrared microscopy," Science **285**, 1224 (1999).
[42]P. Tidemand-Lichtenberg and C. Pedersen, "Long-wavelength, high-resolution microscopy using upconversion in ultra-thin crystals," APL Photonics **9**, 096102 (2024).
[43]J. Fang *et al.*, "Wide-field mid-infrared hyperspectral imaging beyond video rate," Nat. Commun. **15**, 1811 (2024).

06 November 2026 21:33:27

© Author(s) 2026